Selective filtering of excitatory inputs to nucleus accumbens by dopamine and serotonin

Daniel J. Christoffel[a,1], Jessica J. Walsh[a,1], Paul Hoerbelt[a,1], Boris D. Heifets[a,b], Pierre Llorach[b], Ricardo C. Lopez[a], Charu Ramakrishnan[c], Karl Deisseroth[c,d,e], and Robert C. Malenka[a,2]

[a]Nancy Pritzker Laboratory, Department of Psychiatry and Behavioral Sciences, Stanford University, Stanford, CA 94305; [b]Department of Anesthesiology, Perioperative and Pain Medicine, Stanford University School of Medicine, Stanford, CA 94305; [c]Department of Bioengineering, Stanford University, Stanford, CA 94305; [d]Department of Psychiatry and Behavioral Sciences, Stanford University, Stanford, CA 94305; and [e]HHMI, Stanford University, Stanford, CA 94305

Contributed by Robert C. Malenka, May 7, 2021 (sent for review April 7, 2021; reviewed by Antonello Bonci and Mark John Thomas)

The detailed mechanisms by which dopamine (DA) and serotonin (5-HT) act in the nucleus accumbens (NAc) to influence motivated behaviors in distinct ways remain largely unknown. Here, we examined whether DA and 5-HT selectively modulate excitatory synaptic transmission in NAc medium spiny neurons in an input-specific manner. DA reduced excitatory postsynaptic currents (EPSCs) generated by paraventricular thalamus (PVT) inputs but not by ventral hippocampus (vHip), basolateral amygdala (BLA), or medial prefrontal cortex (mPFC) inputs. In contrast, 5-HT reduced EPSCs generated by inputs from all areas except the mPFC. Release of endogenous DA and 5-HT by methamphetamine (METH) and (±)3,4-methylenedioxymethamphetamine (MDMA), respectively, recapitulated these input-specific synaptic effects. Optogenetic inhibition of PVT inputs enhanced cocaine-conditioned place preference, whereas mPFC input inhibition reduced the enhancement of sociability elicited by MDMA. These findings suggest that the distinct, input-specific filtering of excitatory inputs in the NAc by DA and 5-HT contribute to their discrete behavioral effects.

neuromodulators | reward | nucleus accumbens | dopamine | serotonin

The nucleus accumbens (NAc), a major node of classic mesolimbic reward circuitry, plays a critical role in a variety of adaptive and pathological motivated behaviors by integrating information carried by inputs from a broad range of brain areas with distinct, yet overlapping functions (1–6). Output from the NAc is provided by medium spiny neurons (MSNs), the activity of which strongly depends on excitatory inputs from these brain areas, most prominently the ventral hippocampus (vHip), periventricular thalamus (PVT), basolateral amygdala (BLA), and medial prefrontal cortex (mPFC) (3, 7–11). The NAc is also a behaviorally important target for two of the brain's major neuromodulatory systems, dopamine (DA) and serotonin (5-HT) (1, 5, 6, 12–14). DA release in the NAc, whether caused by drugs of abuse or optogenetic stimulation, is powerfully reinforcing and plays a critical role in shaping operant responses (1, 4–6, 15–17). In contrast, unlike DA release, release of 5-HT in the NAc, generated either pharmacologically or optogenetically, is not acutely reinforcing but can powerfully influence sociability (18, 19).

The robust differences in the behavioral consequences of DA and 5-HT release in the NAc suggest that these neuromodulators must influence MSN activity in, perhaps profoundly, different ways. Yet little is known about the detailed mechanisms by which these neuromodulators accomplish this task. Because of the importance of excitatory input in controlling MSN activity and the fact that both DA and 5-HT are well established to modulate excitatory synaptic transmission in the NAc (18, 20–23), we hypothesized that an important mechanism by which these neuromodulators might distinctly influence MSN activity is by differentially filtering incoming information from major input structures. Specifically, we hypothesized that DA and 5-HT would depress excitatory synaptic transmission in distinct, input-specific manners. Because of methodological limitations prior to the advent of optogenetics, virtually all previous work examining DA and 5-HT modulation of excitatory transmission in the NAc used bulk electrical stimulation of unknown inputs.

Consistent with our hypothesis, exogenously applied DA and 5-HT, as well as release of endogenous DA and 5-HT, depressed excitatory synaptic transmission in distinct, input-specific manners. Input-specific optogenetic inhibition of excitatory inputs to the NAc revealed input-specific effects on conditioned place preference and sociability assays, which are affected by NAc release of DA and 5-HT, respectively. Together, these results provide evidence that the input-specific filtering of excitatory input from distinct brain regions contributes to the behavioral effects of DA and 5-HT release in the NAc and provides a foundation for further work elucidating the neural mechanisms by which modulation of NAc activity influences motivated behaviors.

Results

Excitatory Input Connectivity onto D1-MSNs Using Dual Input Activation. In initial experiments, adeno-associated viruses (AAVs) expressing

Significance

Dopamine (DA) and serotonin (5-HT) release in the nucleus accumbens (NAc) influence motivated behaviors, yet the mechanisms by which they modulate NAc activity are unclear. Here, we report that DA selectively reduced excitatory postsynaptic currents (EPSCs) from paraventricular thalamus (PVT) inputs, whereas 5-HT reduced EPSCs from PVT, ventral hippocampus (vHip), and basolateral amygdala (BLA) inputs but not medial prefrontal cortex (mPFC) inputs. Mimicking the input-specific effect of DA via optogenetic inhibition of the PVT promoted cocaine-conditioned place preference, while inhibition of the mPFC blocked the enhancement of sociability induced by (±)3,4-methylenedioxymethamphetamine (MDMA). Together, these results suggest that these input-specific effects on NAc excitatory transmission contribute to the distinct modulation of behavior that is generated by release of DA and 5-HT.

Author contributions: D.J.C., P.H., and B.D.H. performed and analyzed electrophysiological experiments; P.H. designed AAV plasmids; J.J.W. and P.H. conducted all surgeries; D.J.C. and R.C.L. made all optogenetic implants; D.J.C., J.J.W., and P.L. performed and analyzed behavioral studies; C.R. and K.D. designed and supplied the plasmid for the -NRN constructs; and D.J.C., J.J.W., P.H., and R.C.M. designed the project and wrote the paper with contributions from all authors.

Reviewers: A.B., Global Institutes on Addiction; and M.J.T., University of Minnesota Health.

Competing interest statement: R.C.M. is on the scientific advisory boards for MapLight Therapeutics and MindMed. K.D. is on the scientific advisory board of MapLight Therapeutics.

[1]D.J.C., J.J.W., and P.H. contributed equally to this work.

[2]To whom correspondence may be addressed. Email: malenka@stanford.edu.

This article contains supporting information online at https://www.pnas.org/lookup/suppl/doi:10.1073/pnas.2106648118/-/DCSupplemental.

Published June 8, 2021.

the opsin Chronos (blue-light activated) or ChrimsonR (red-light activated) (24) were injected into the mPFC of male and female D1-tdTomato bacterial artificial chromosome (BAC) transgenic mice (25) (*SI Appendix*, Fig. S1*A*). Since DA and 5-HT are thought to affect excitatory transmission primarily through a presynaptic mechanism (20–23, 26, 27), we recorded only from D1-MSNs in the NAc medial shell because, compared with D2-MSNs, they appear to express greater input-selective synaptic plasticity following administration of psychostimulants (28–31). Whole-cell voltage clamp recordings from visually identified D1-MSNs in the NAc were obtained from acute coronal slices (*SI Appendix*, Fig. S1 *B* and *C*). In Chronos-infected mice, whole-field blue (470 nm), but not red (595 nm), light illumination evoked excitatory postsynaptic currents (EPSCs) that scaled with increasing light power (*SI Appendix*, Fig. S1*B*; $n = 10$ cells, 2 mice). Similarly, as expected, in ChrimsonR-infected mice, only red-light illumination evoked reliable EPSCs, the sizes of which were also dependent on light power (*SI Appendix*, Fig. S1*C*) ($n = 8$ cells, 4 mice).

To further test possible cross talk between blue and red light activation of Chronos and ChrimsonR, respectively, we injected AAVs expressing Chronos into the vHip and AAVs expressing ChrimsonR into the PVT (*SI Appendix*, Fig. S1 *A* and *D*). We then analyzed the paired-pulse ratio (PPR; amplitude of $EPSC_2$/$EPSC_1$; 50 ms interstimulus interval) of each input using two different conditions: 1) the same wavelength light for both pulses, which generates a simple form of presynaptic short-term plasticity (*SI Appendix*, Fig. S1*E*) (32); and 2) a different wavelength for each evoked EPSC. Same-wavelength stimulation generated either a paired-pulse facilitation or paired-pulse depression (*SI Appendix*, Fig. S1*E*; $n = 7$ cells, 5 mice), presumably because the same set of synapses was stimulated twice. In contrast, $EPSC_2$ was unaffected when the different wavelength was used to generate $EPSC_1$ (*SI Appendix*, Fig. S1*E*). Together, these experiments confirm that it is possible to express Chronos and ChrimsonR in different brain regions that send inputs to NAc and use different wavelengths of light to activate these inputs independently.

To assess input connectivity and maximize the likelihood of being able to generate EPSCs in NAc D1-MSNs from a known input, we used the protocol just described (expressing Chronos in vHip and ChrimsonR in PVT) or, instead, expressed Chronos in BLA and ChrimsonR in mPFC (*SI Appendix*, Fig. S1*A*). In the animals in which AAVs were injected into vHip and PVT ($n = 52$ mice), virtually all D1-MSNs ($n = 160$ of 163 cells) expressed detectable EPSCs (>10 pA) from at least one of the two activated inputs, with 55% of these cells generating EPSCs from both sets of inputs (*SI Appendix*, Fig. S1*F*). For animals in which AAVs were injected into BLA and mPFC ($n = 10$ mice), again, virtually all D1-MSNs ($n = 26$ of 27 cells) generated EPSCs from one of the inputs, with 44% generating EPSCs from both inputs (*SI Appendix*, Fig. S1*G*). In a third set of animals in which AAVs were injected into vHip and mPFC ($n = 5$ mice), all D1-MSNs ($n = 19$ of 19 cells) expressed EPSCs from at least one of the inputs, with 47% generating EPSCs from both inputs (*SI Appendix*, Fig. S1*H*). These findings support the prevailing idea that individual MSNs are contacted by multiple converging inputs (3, 4, 22, 33–35).

Input-Specific Depression of Synaptic Transmission by DA and 5-HT. Our connectivity analyses (*SI Appendix*, Fig. S1) suggested that using a two-opsin strategy to activate independent sets of inputs from two different brain regions and record from single NAc MSNs should be fairly routine. However, in practice, it was difficult to generate stable EPSCs for the ∼30 to 40 min required to alternate input stimulation with Chronos and ChrimsonR, obtain stable baselines, and apply DA or 5-HT. This may be due to the cations entering presynaptic terminals via these opsins or some feedback or feedforward modulation of one input by the other. Thus, to compare the effects of DA or 5-HT on optically evoked EPSCs generated by inputs from vHip, PVT, BLA, and mPFC, activation of only one of the expressed opsins was used routinely.

Application of DA to NAc slices is known to modestly depress excitatory synaptic transmission in MSNs when EPSCs are generated by unknown inputs activated by electrical stimulation (21, 22, 26, 36–39). Surprisingly, when EPSCs were generated by optogenetic activation of known inputs, DA (50 μM) application robustly depressed EPSCs generated by PVT inputs (Fig. 1*A*; 40.5 ± 7.3% depression, $n = 10$) but had minimal effects on EPSCs generated by vHip (Fig. 1*B*; $n = 16$), BLA (Fig. 1*C*; $n = 8$) or mPFC inputs (Fig. 1*D*; $n = 8$). Thus, DA appears to preferentially filter inputs from PVT and not detectably influence the three other major NAc inputs.

Application of 5-HT to NAc slices also depresses EPSCs generated by unknown inputs to NAc MSNs (18, 20, 23, 27). Strikingly, the inputs affected by 5-HT were dramatically different from those influenced by DA. Application of 5-HT (5 μM) reliably depressed EPSCs generated by inputs from PVT (Fig. 1*E*; 46.4 ± 7.0%, $n = 6$), vHip (Fig. 1*F*; 33.5 ± 6.0%, $n = 12$), and BLA (Fig. 1*G*; 43.3 ± 7.1%, $n = 9$). Yet EPSCs generated by mPFC inputs to NAc D1-MSNs were minimally affected (Fig. 1*H*; $n = 6$). A summary of these results (Fig. 1 *I* and *J*) illustrates the differences in how DA and 5-HT filtered excitatory synaptic transmission at four major inputs to the NAc. DA preferentially inhibits PVT inputs, while 5-HT preferentially spares mPFC inputs.

Despite the difficulties in using the two-opsin strategy, in a subset of cells, we were able to perform this experimental procedure and replicate the results obtained in experiments when only a single input at a time was activated. Specifically, DA depressed transmission at PVT→NAc D1-MSN synapses while not affecting EPSCs generated in the same cell at vHip→NAc synapses (*SI Appendix*, Fig. S2*A*; $n = 7$). While 5-HT depressed EPSCs generated at BLA→NAc D1-MSN synapses, it had no consistent effect on the EPSCs generated by mPFC inputs in the same cell (*SI Appendix*, Fig. S2*B*; $n = 3$). These results provide further evidence that DA and 5-HT distinctly modulate excitatory inputs to NAc D1-MSNs.

To test the hypothesis that DA and 5-HT modulate excitatory synaptic transmission in the NAc primarily by acting presynaptically to reduce glutamate release (20–23, 26, 27), in a subset of experiments, we used input-specific stimulation to calculate PPRs (50 ms interstimulus interval). PPRs of EPSCs generated by PVT inputs were increased by DA (*SI Appendix*, Fig. S3*A*; $n = 10$), while PPRs of EPSCs generated by vHip, PVT, and BLA inputs were increased by 5-HT (*SI Appendix*, Fig. S3 *B–D*; $n = 5$ to 12). Additionally, under our recording conditions, application of these modulators had no significant effects on series resistances or postsynaptic membrane resistances (*SI Appendix*, Fig. S3 *E–H*). These results support the conclusion that DA and 5-HT modulate excitatory synaptic transmission in the NAc primarily by acting presynaptically.

Input-Specific Depression of Synaptic Transmission by Methamphetamine and (±)3,4-methylenedioxymethamphetamine. A critical question is whether endogenous DA and 5-HT will influence EPSCs in the same input-specific manner as exogenously applied DA and 5-HT. To address this question, we used (+)methamphetamine (METH) to preferentially release DA and (±)3,4-methylenedioxymethamphetamine (MDMA) to preferentially release 5-HT (40). Amphetamines have been shown to depress excitatory synaptic transmission in NAc MSNs when unknown inputs were stimulated, due to the release of the respective neuromodulators (18, 26, 39, 41). Bath application of METH (5 μM) closely mimicked the effects of DA application, depressing EPSCs generated by PVT inputs (Fig. 2*A*; 34.1 ± 7.9% depression, $n = 6$) while, like DA, minimally effecting EPSCs generated by vHip (Fig. 2*B*; $n = 10$), BLA (Fig. 2*C*, $n = 6$), and mPFC inputs (Fig. 2*D*, $n = 10$). Prior application of the broad DA-receptor antagonist flupenthixol blocked

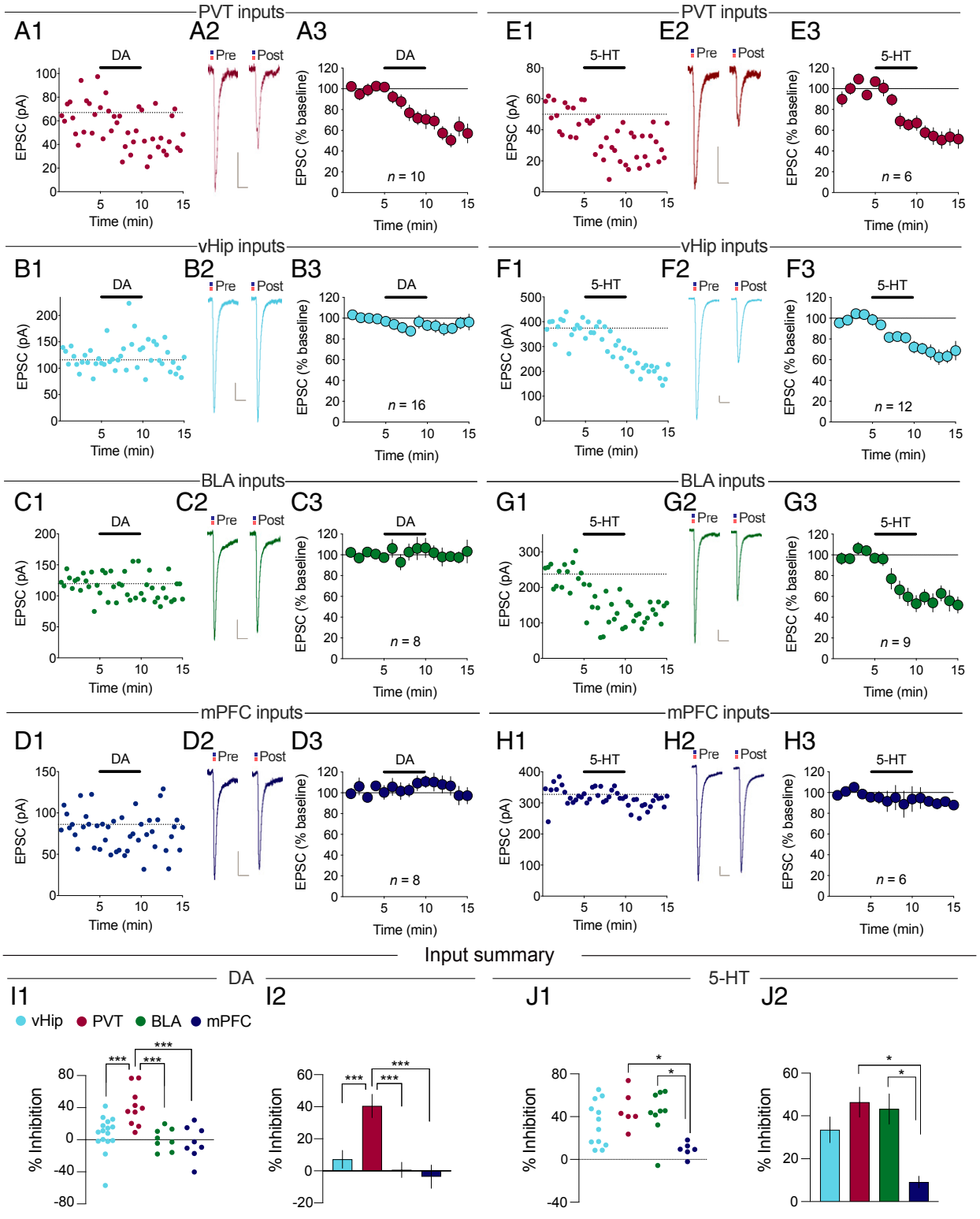

Fig. 1. Input-specific depression of excitatory transmission by DA and 5-HT. (*A*) Effect of DA on PVT→NAc D1-MSN EPSCs. (A_1) Example experiment. (A_2) Sample averaged traces ($n = 15$ EPSCs) pre- and post-DA application. (Scale bars: 20 ms/20 pA.) (A_3) Summary of all experiments (mean ± SEM). (*B–H*) Same as *A* for DA (*B–D*) or 5-HT (*E–H*) acting on EPSCs generated by vHip (*B* and *F*), BLA (*C* and *G*), or mPFC (*D* and *H*) inputs. (*I*) Summary of EPSC inhibition caused by DA ($F_{4,64} = 7.008$, $P < 0.001$) or (*J*) 5-HT ($F_{4,50} = 2.988$, $P < 0.05$) Mean ± SEM *$P < 0.05$, ***$P < 0.001$, one-way ANOVA with Holm–Šidák multiple comparisons. See also *SI Appendix*, Figs. S2 and S3.

METH-induced depression of EPSCs from PVT inputs (*SI Appendix*, Fig. S4*A*; $n = 5$), thereby confirming that this effect of METH was via DA receptors. On the other hand, MDMA (10 μM), like 5-HT, depressed EPSCs generated by activation of inputs from PVT (Fig. 2*E*; 37.1 ± 4.0%, $n = 6$), vHip (Fig. 2*F*; 29.4 ± 6.0%, $n = 10$), and BLA (Fig. 2*G*; 29.0 ± 6.4%, $n = 9$) but had no effect on EPSCs generated by mPFC inputs (Fig. 2*H*, $n = 8$). Furthermore, the MDMA-induced depression of EPSCs from PVT inputs was not affected by pretreatment with flupenthixol (*SI Appendix*, Fig. S4*B*; $n = 3$), whereas prior application of the 5-HT1b receptor antagonist NAS-181 completely blocked MDMA-induced depression at vHip inputs, confirming this effect of MDMA was via presynaptic 5-HT1b receptors (*SI Appendix*, Fig. S4*C*; $n = 6$). The summary of these results (Fig. 2 *I* and *J*) demonstrates that the actions of DA and 5-HT on input-specific filtering of excitatory synaptic transmission in NAc D1-MSNs were precisely mimicked by METH and MDMA, respectively.

Behavioral Consequences of Input-Specific Inhibition in NAc. To address if the input-specific filtering of excitatory inputs to NAc by DA and 5-HT might have behavioral relevance, we next examined the behavioral consequence of inhibiting each of the four inputs to NAc by expressing halorhodopsin 3.0 (NpHR) or, as a control, eYFP, in the BLA, vHip, mPFC, or PVT and stimulating NpHR via fiber implants in the NAc (*SI Appendix*, Fig. S5*A*). Blinded to the expressed transgene, we performed behavioral tests focusing on assays that are robustly influenced by the release of DA and 5-HT in the NAc (*SI Appendix*, Fig. S5*B*). In contrast to manipulations that release DA in the NAc (1, 5, 15, 16, 42), inhibition of BLA, vHip, mPFC, or PVT inputs to NAc had no consistent effect in a conditioned place preference (CPP) assay (Fig. 3 *A–D*) and did not affect time spent exploring a novel object, locomotor activity, or center time in an open field ($n = 18$ to 24 mice in each group; *SI Appendix*, Fig. S5 *C–F*). Since DA's rewarding effects may be due to its action at multiple loci in the NAc, and because activation of PVT→NAc inputs can be aversive (9), we next tested if inhibition of these inputs might enhance the reinforcing properties of an experience, which alone is a subthreshold for eliciting CPP (Fig. 3*E*; cocaine at 5 mg/kg) (43). Consistent with this prediction, inhibiting PVT→NAc inputs using NpHR during the conditioning sessions resulted in the development of a cocaine CPP ($n = 17$), which did not occur in animals expressing eYFP in the PVT ($n = 16$; Fig. 3*F*).

Release of 5-HT in the NAc promotes social approach in the three-chamber and juvenile-intruder sociability assays (18, 19). While inhibition of BLA→NAc inputs with NpHR mimicked these effects (Fig. 4*A*), surprisingly, inhibition of vHip→NAc inputs reduced sociability in both assays (Fig. 4*B*). In contrast, inhibition of mPFC→NAc inputs and PVT→NAc inputs had no consistent effects on sociability (Fig. 4 *C* and *D*). To test if the lack of effect of 5-HT on mPFC→NAc synaptic transmission is important for the enhancement of sociability elicited by 5-HT release in the NAc (19), we administered MDMA, which enhances social preference in the three-chamber assay due to NAc 5-HT release (18), and inhibited mPFC→NAc input activity with NpHR (Fig. 4*E*). In eYFP-expressing animals, light stimulation in the NAc had no effect on the MDMA-induced enhancement of social preference, while the same stimulation in NpHR expressing animals blocked the prosocial effects of MDMA (Fig. 4*F*).

Discussion

Using optogenetics to selectively activate major excitatory inputs to the NAc, we found that DA preferentially depresses PVT→NAc excitatory synaptic transmission, while 5-HT preferentially spares mPFC →NAc transmission. METH and MDMA recapitulated the effects of exogenous DA and 5-HT, respectively, providing evidence that endogenous release of these modulators has the same synaptic effects. The potential behavioral consequences of this distinct input-selective filtering of incoming information by DA and 5-HT were assayed by input-specific optogenetic inhibition experiments. Although inhibition of each of the inputs did not elicit detectable effects in a CPP assay or several control behaviors, inhibition of PVT→NAc inputs enhanced the rewarding effects of a subthreshold dose of cocaine assessed with CPP, a well-established consequence of releasing DA in the NAc (5, 15, 16). In contrast, inhibition of mPFC→NAc inputs reduced the MDMA-induced enhancement of social approach, a result consistent with the powerful effects of 5-HT release in the NAc on sociability (18, 19, 44, 45).

There are several possible mechanisms that might account for the input-specific effects of DA and 5-HT. The most parsimonious explanation is that the receptors mediating the synaptic effects of these modulators are preferentially located on the presynaptic terminals of inputs from specific brain regions. For 5-HT, this would mean that presynaptic 5-HT1b receptors, which are well established to mediate the synaptic depression caused by 5-HT in the dorsal and ventral striatum (18–20, 23), are found on inputs from vHip, BLA, and PVT but not those from mPFC. For DA, the situation is more complex. Previous work consistently reported that D1-receptor antagonists block the synaptic effects of DA in the NAc (26, 39, 46). However, recent work (46) suggests that the critical D1-receptors are found on astrocytes, which release ATP/adenosine that in turn activates presynaptic A1-receptors to depress excitatory synaptic transmission. This hypothesis is consistent with previous work also suggesting that the effects of DA on excitatory transmission in the NAc are mediated by adenosine (38). If this mechanism applies to our experiments, the selective inhibition of PVT→NAc transmission could be due to the preferential location of A1 receptors on PVT inputs. Alternatively, the input-specific effects of DA might be due to a specialized anatomical arrangement between DA release sites and PVT input synapses on NAc MSNs. Consistent with this possibility, ultrastructural studies revealed close apposition between PVT terminals in the NAc shell and tyrosine hydroxylase-positive axons (47). An important limitation of these experiments is that recordings were made only from D1-MSNs. In future studies, it will be important to determine if the synaptic responses in D2-MSNs are modulated by DA and 5-HT in the same input-specific manner.

The other major question our results raise is whether selective inhibition of specific excitatory inputs contributes to the behavioral consequences of DA and 5-HT release in the NAc. While activation of most excitatory inputs to NAc have been reported to be reinforcing (1, 10, 11, 48), activation of PVT→NAc inputs generated real-time place aversion (9). Based on these results, the simplest explanation for our finding that inhibition of PVT→NAc inputs enhanced the reinforcing properties of cocaine is that this manipulation generates a form of negative reinforcement by relieving aversive experience due to PVT→NAc input activity. That the inhibition of PVT→NAc input activity alone did not elicit CPP, which NAc DA release reliably generates (5, 15–17, 49), indicates that the powerful reinforcing consequences of NAc DA release requires additional modulatory mechanisms in the NAc such as differential effects on the excitability of D1- and D2-MSNs. Alternatively, it is possible that the NpHR-mediated inhibition of excitatory synaptic inputs was not sufficiently strong to elicit the degree of "reward" that is necessary to evoke CPP.

The effect of input-specific inhibition of excitatory inputs to the NAc on sociability was more complicated. Inhibition of BLA→NAc inputs enhanced, while inhibition of vHip→NAc reduced, social preference and approach. Importantly, inhibition of mPFC→NAc inputs decreased the enhancement of social preference elicited by MDMA. These results are not easy to reconcile with the simple hypothesis that NAc 5-HT release promotes sociability due solely to its input-specific filtering of excitatory inputs

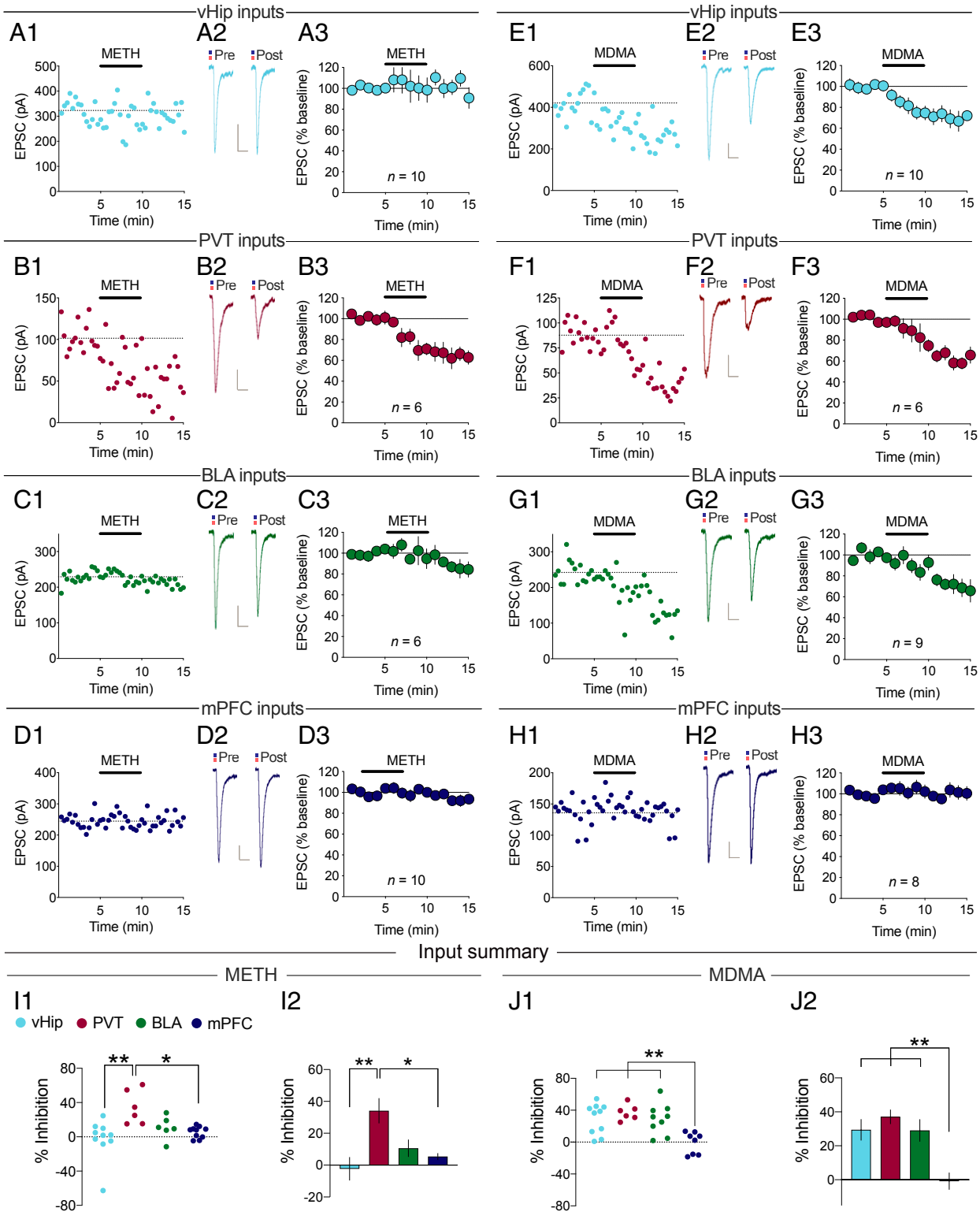

Fig. 2. METH and MDMA recapitulate DA and 5-HT actions. (*A*) Effect of METH on PVT→NAc D1-MSN EPSCs. (A_1) Example experiment. (A_2) Sample averaged traces (n = 15 EPSCs) pre- and post-METH application. (Scale bars: 20 ms/20 pA.) (A_3) Summary of all experiments (mean ± SEM). (*B–H*) Same as *A* for METH (*B–D*) or MDMA (*E–H*) acting on EPSCs generated by vHip (*B* and *F*), BLA (*C* and *G*), or mPFC (*D* and *H*) inputs. (*I*) Summary of EPSC inhibition caused by METH ($F_{4,44} = 4.815$, $P < 0.01$) or (*J*) MDMA ($F_{4,54} = 4.750$, $P < 0.01$). Mean ± SEM *$P < 0.05$, **$P < 0.01$, one-way ANOVA with Holm–Šidák multiple comparisons. See also *SI Appendix*, Fig. S4.

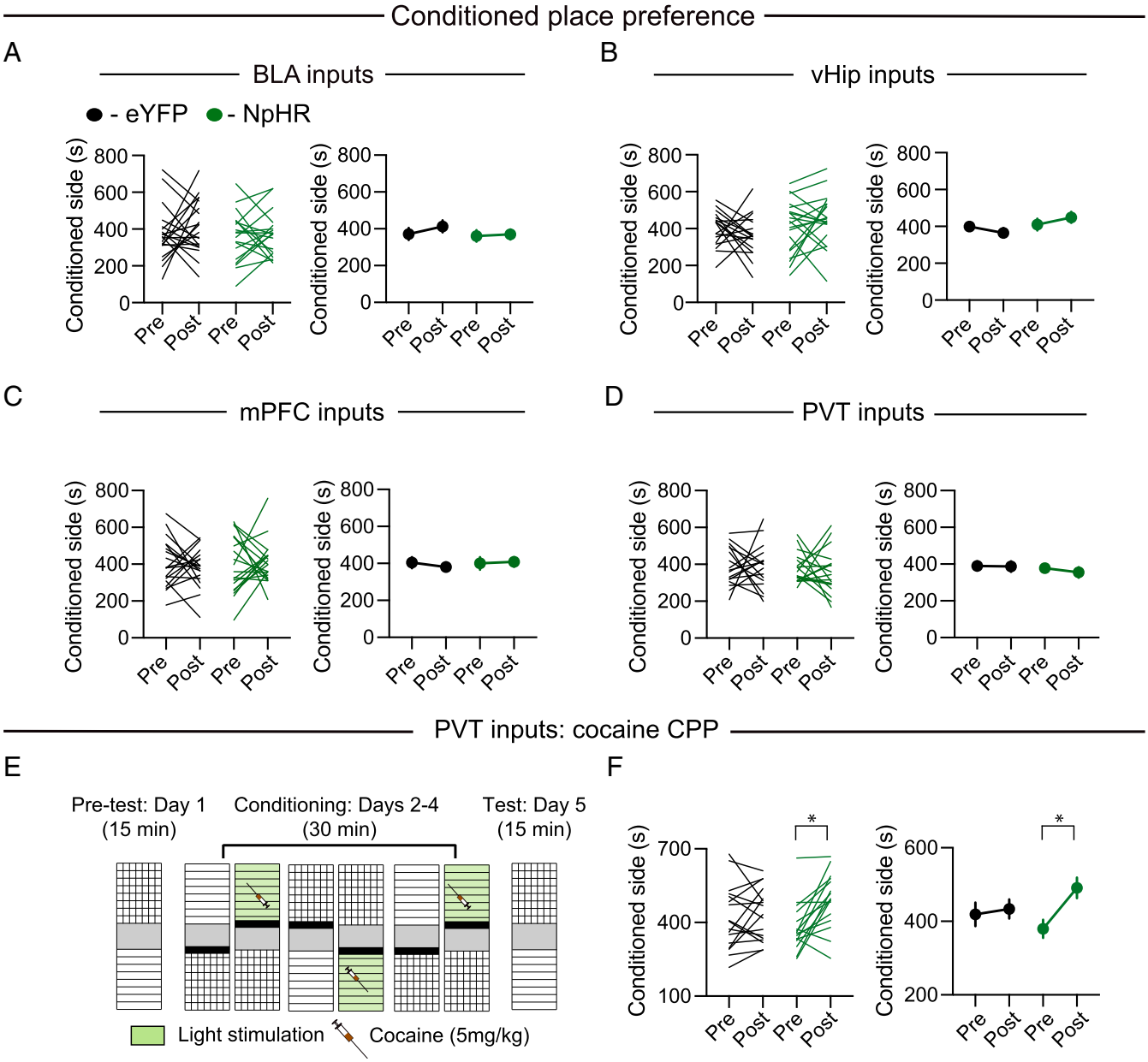

Fig. 3. Effects of input-specific inhibition in NAc on CPP. (*A–D*) Effects of inhibition of BLA, vHip, mPFC, and PVT inputs to NAc on CPP (left graphs illustrate individual subjects; right graphs display mean ± SEM). (*E*) Cocaine CPP schematic. (*F*) Effects of PVT→NAc inhibition on subthreshold cocaine CPP ($F_{1,31} = 6.53$, $P < 0.05$). *$P < 0.05$; two-way ANOVA with Šidák's multiple comparison post hoc test. See also *SI Appendix*, Fig. S5.

from BLA, vHip, and PVT but not mPFC. However, they are consistent with an important role for such input-specific modulatory effects as well as previous results examining the effects of NAc inputs on social behaviors. Specifically, optogenetic activation of BLA inputs to NAc reduced sociability, whereas inhibition promoted social interaction in *Shank3B*$^{-/-}$ mice (50). Furthermore, that sparing mPFC→NAc input activity is necessary for the effects of NAc 5-HT release on sociability is consistent with reports that mPFC→NAc circuit activity promotes social bonding in prairie voles (51), mPFC neuron activity in mice correlates with social approach (52), and social avoidance in stressed mice can be reversed by activating mPFC neurons (53). Although activation of inputs from the prelimbic cortex to the NAc core was reported to decrease social preference (54), this specific circuit may encode and participate in markedly different behaviors than the mPFC projections to the medial shell (55–58), which arise mainly from infralimbic (as opposed to prelimbic) mPFC in rodents (59, 60).

The demonstration of the distinct input-specific effects of DA and 5-HT on excitatory transmission is a first step toward a comprehensive understanding of the mechanisms by which DA and 5-HT modify NAc circuit activity to mediate their complex behavioral effects. Much more work will be required to address the many questions that remain to be answered (1, 61). For example, do individual NAc MSNs show functionally important heterogeneity in their input and output connectivity? Our findings that individual NAc D1-MSNs were frequently contacted by inputs from multiple brain regions is consistent with the generally accepted hypothesis that inputs from multiple brain regions can converge onto single NAc MSNs (3, 4, 22, 33, 34). However, many details about this convergence are unknown. Another key issue is whether DA and 5-HT are released in the same NAc

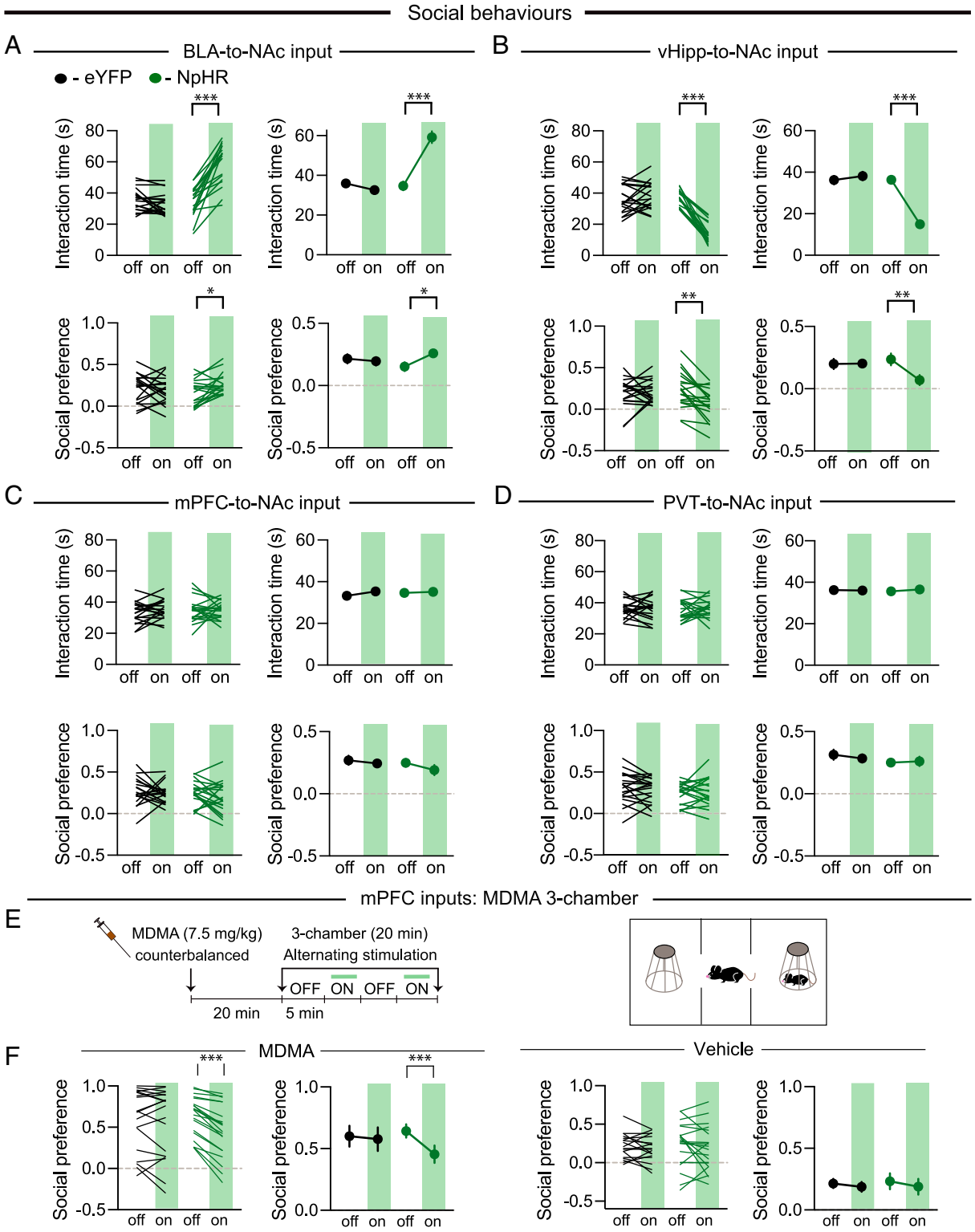

Fig. 4. Effects of input-specific inhibition in NAc on sociability. (*A–D*) Effects of inhibition of BLA, vHip, mPFC, and PVT inputs to NAc on juvenile interaction and three-chamber sociability (green shading indicates optical inhibition). (*A*, *Top*) $F_{1,37} = 72.46$, $P < 0.001$, (*A*, *Bottom*) $F_{1,37} = 5.936$, $P < 0.05$. (*B*, *Top*) $F_{1,37} = 79.84$, $P < 0.01$, (*B*, *Bottom*) $F_{1,37} = 8.591$, $P < 0.01$. (*E*) Timeline and schematic of MDMA three-chamber assay. (*F*) Effects of mPFC→NAc inhibition on MDMA-induced enhanced social preference ($F_{1,37} = 15.38$, $P < 0.001$). ***$P < 0.001$; two-way ANOVA with Šidák's multiple comparison post hoc test.

subregions and whether they influence activity in the same populations of MSNs or nonoverlapping populations. A third important topic concerns the physiological effects of endogenously released DA and 5-HT on the different subtypes of neurons in the NAc (e.g., D1-MSNs versus D2-MSNs; patch neurons versus matrix neurons). Clearly, a daunting amount of work will be required to achieve a comprehensive mechanistic understanding of how DA and 5-HT action in the NAc generate such robust

behavioral effects. We hope that the results presented here provide foundational knowledge that can be greatly expanded by application of the armamentarium of new techniques now available to neuroscientists.

Materials and Methods

Animals. Adult male and female mice, at least 10 wk old, were used for all experiments following AAV injections in animals >4 wk old for electrophysiology and >6 wk old for behavioral experiments. C57BL/6J mice (Jackson, stock # 000664) were used for behavioral experiments. Juveniles (3 to 5 wk old) of the same strain and sex were used for sociability assays. To identify D1-MSNs during electrophysiology recordings, hemizygous offspring of Drd1a-tdTomato/Drd2-EGFP BAC double transgenic mice backcrossed to wild-type C57BL/6J mice were used. All mice were group-housed on a 12-h light/dark cycle (lights on at 7:00 AM) with food and water ad libitum. Behavioral experiments were conducted between 8:00 AM and 6:00 PM. All procedures were in compliance with NIH animal care standards and were approved by Stanford University's Administrative Panel on Laboratory Animal Care and Administrative Panel on Biosafety.

Stereotactic Surgery. Surgeries were performed in a sterile, temperature-controlled environment. Mice were anesthetized with inhaled isoflurane (IsoThesia, Henry Schein) (1 to 2%) and placed into a stereotactic head frame (Kopf Instruments, Model 940). The skull surface was exposed, and craniotomy holes for AAV injections or fiber optic implants were drilled with a 0.5-mm fine bit (Fine Science Tools, 19007-05). In mice scheduled for behavioral experiments, implants were held to the skull with two screws in the parietal bones, secured with sequentially applied Metabond (Parkell) and Dual Cure Resin Ionomer (DenMat, Geristore, no. 4506). Local anesthetic (lidocaine 0.5%, APP Pharmaceuticals, LLC) was injected into the scalp incision, and meloxicam (Boehringer Ingelheim Vetmedica, Inc., 5 mg/kg subcutaneous) was given for postoperative analgesia. In mice scheduled for electrophysiology experiments, Vetbond (3M) was used to secure the scalp closed.

AAV Injections. Syringes (Hamilton, Model 85 RN SYR) with 33-gauge needles (VWR, no. 7762) were used to bilaterally inject 500 nl AAV per side into craniotomy holes at the following coordinates (from Bregma, in mm):

vHip: AP: −3.3, ML: ±3.0, DV: −4.0.
PVT: AP: −1.2, ML: 0.0, DV: −3.0.
BLA: AP: −1.2, ML: ±2.8, DV: −4.7.
mPFC: AP: +1.7, ML: ±0.3, DV: −2.7.

AAVs were infused at 100 nl/min for 5 min; then the injection needle was held in place for 5 min before slowly withdrawing to prevent leakage and tissue damage. AAVs used in this study were used undiluted (titers from 10^{12} to 10^{14} vg/mL) and consisted of AAV-DJ-hSyn-Chronos-mT-Sapphire and AAV-DJ-hSyn-ChrimsonR-LSSmOrange for electrophysiology studies [or AAV8-hSyn-Chronos-mT-Sapphire-NRN and AAV8-ChrimsonR-LSSmOrange-NRN for some experiments (62), which produced identical results]. Behavioral experiments used AAV8-CamKIIα-NpHR 3.0-eYFP and AAV8-CamKIIα-eYFP. All AAVs were supplied by the Stanford Neuroscience Gene Virus and Vector Core (GVVC). Behavior and electrophysiology experiments were conducted >7 wk after AAV injection.

Generation of AAVs. Standard subcloning procedures were followed to generate pAAV-hSyn-Chronos-mT-Sapphire (-NRN) and pAAV-hSyn-ChrimsonR-LSSmOrange (-NRN) plasmids for electrophysiology experiments. The following plasmids were purchased from Addgene: catalog numbers 37131 (pLSSmOrange-C1), 54545 (mT-Sapphire-C1), 58806 (pAAV-Syn-ChrimsonR-GFP), and 59170 (pAAV-Syn-Chronos-GFP). Briefly, chemically competent *Escherichia coli* (One Shot Stbl3 cells, ThermoFisher catalog # C737303) were used to grow circular plasmids, which were then selected on ampicillin- or kanamycin-infused culture plates at 37 °C. The placement of insertions was ensured using the Gibson assembly technique: overhanging primers (Elim Biopharm) were generated, PCR was conducted with T4 DNA polymerase (New England Biolabs [NEB]), and gel purification/extraction (Qiagen) was done on 0.8% agarose gel. Following ligation with DNA ligase (NEB), transformation into Stbl3 *E. coli*, and miniprep (Qiagen), insertions were verified using restriction enzymes (NEB), and plasmids were maxiprepped (Qiagen). Purified plasmids were packaged into AAVs by the Stanford Neuroscience GVVC.

Optical Fiber Implants. For behavioral experiments, bilateral optical fiber implants (200 μm thick, custom cut, Thorlabs, FT200EMT fiber with CFLC230-10 ferrule and glued with Blue Dye Epoxy, T60-065-B2) were lowered through craniotomy holes, placed just above the NAc medial shell, and permanently secured (see *Stereotactic Surgery* section). Bregma coordinates were (in mm): AP: +1.6, ML: ±1.5, DV: −4.2, 10° angle.

Electrophysiology. Whole-cell voltage clamp recordings were conducted >8 wk after AAV injection. Mice were deeply anesthetized with isoflurane, perfused intracardially with ice-cold artificial cerebrospinal fluid (aCSF), and then 250-μm coronal slices containing the NAc medial shell were cut into ice-cold sucrose solution with a vibratome (Leica VT1200S). aCSF contained the following (in mM): 126 NaCl, 3 KCl, 1 Na_2HPO_4, 26.2 $NaHCO_3$, 2.5 $CaCl_2{\bullet}2H_2O$, 1.3 $MgSO_4{\bullet}7H_2O$, 11 D-glucose (~7.3 pH, 295 to 305 mOsm) and oxygenated with 95% O_2/5% CO_2. Sucrose (cutting) solution contained the following (in mM): 230 sucrose, 2.5 KCl, 1.25 NaH_2PO_4, 24 $NaHCO_3$, 0.5 $CaCl_2{\bullet}2H_2O$, 7 $MgSO_4{\bullet}7H_2O$, 11 glucose (~7.3 pH, ~320 mOsm) and oxygenated with 95% O_2/5% CO_2.

After recovering for 60 min in oxygenated aCSF at 33 °C, slices were transferred to a recording chamber and perfused at 2 to 4 mL with oxygenated aCSF at 30 °C for experiments. Recording aCSF always contained 100 μM picrotoxin (Sigma-Aldrich) to block $GABA_A$-evoked currents. DA (50 μM) and 5-HT (5 μM) were made up fresh on the day of the experiment, whereas METH (+ enantiomer) (5 μM), MDMA (± enantiomer) (10 μM), flupenthixol (20 μM), and NAS-181 (20 μM) were diluted 1:1,000 from stocks stored at −20 °C. All compounds were hydrochloride salts from Sigma-Aldrich dissolved in water (stocks) or aCSF (day of experiment). For experiments with DA, aCSF contained 1 mM ascorbic acid or 50 μM sodium metabisulfite (both from Sigma-Aldrich) to prevent oxidation of DA, which did not affect recordings otherwise. Recordings were conducted with pulled borosilicate glass (G150TF-4, Warner Instruments) patch pipettes (2.5 to 5.5 MΩ) filled with internal solution containing the following (in mM): 130 $CsMeSO_3$, 10 Hepes, 0.4 EGTA, 5 tetraethylammonium chloride (TEA-Cl), 7.5 Na_2phosophocreatine, 4 MgATP, 0.4 NaGTP, 0.1 spermine, 4 QX-314 Br (7.3 pH, 290 to 295 mOsm). D1-MSNs were identified by the presence of tdTomato or the absence of EGFP (63), Chronos was visualized by the presence of mT-Sapphire in input terminals to the NAc, and ChrimsonR was visualized by the presence of LSSmOrange (64) in terminals, viewed through a 40× water-immersion objective on a fluorescence microscope (BX51WI, Olympus) with infrared-differential interference contrast and epifluorescence. Filter cubes were purchased from Semrock or Chroma. Recordings were made with a MultiClamp 700B amplifier (Axon Instruments, Inc.). Output signals were filtered at 4 kHz and digitized at 10 kHz, and neurons were held at −70 mV for voltage clamp recordings. Series resistance (Rs, <30 MΩ) was continuously monitored during recordings, which were terminated if >25% change occurred. Membrane resistance and Rs were monitored and analyzed using a 50-ms, −5 mV pulse every 20 s throughout recordings. All data were acquired and analyzed with Axograph software.

EPSCs were evoked with 5-ms pulses using blue (470 nm) or red (595 nm) light, ranging from 0.2 to 3 mW, delivered through the microscope objective by light-emitting diodes (LEDs) (Thorlabs) (24). For amplitude measurements, EPSCs were evoked 20 s apart, and three EPSC amplitudes were averaged per minute to obtain reported values. For each experiment, a baseline (5 min) was first obtained in which EPSC amplitude did not vary from beginning to end of the baseline period by more than 15%. DA, 5-HT, METH, or MDMA were applied for 5 min and then washed out with aCSF solution. To quantify the change in EPSC after drug application for experiments shown in Figs. 1 and 2, the average EPSC amplitude from 10 to 15 min was calculated, normalized to the baseline average, and then percent inhibition was calculated. For antagonist studies in *SI Appendix*, Fig. S4, flupenthixol or NAS-181 were continuously applied throughout the recording. To separate EPSCs evoked from blue and red light in mice containing both Chronos and ChrimsonR, a PPR protocol was conducted as follows: EPSCs were evoked via light pulses set at 50-ms intervals, and at least five repetitions of the sequence blue–blue, red–red, blue–red, red–blue were performed per neuron. Amplitudes from the five repetitions were then averaged and examined before starting an experiment with that neuron. If the $EPSC_2/EPSC_1$ PPR for alternating colors was between 0.8 and 1.2 (close to 1), the two EPSCs were deemed to be from separate pathways, and the experiment was conducted. If the inputs were not separate, which occurred in 19 of 130 cells, the one input not affected by cross talk was still used for the experiment, but data from the other input was not collected. Light powers were controlled and monitored during all experiments (0.2 to 3 mW) to ensure that observed EPSCs did not arise from cross talk, particularly if same-color PPRs were also within the range of 0.8 and 1.2. Light powers were not adjusted during experiments once set after PPR testing. For a minority of recorded cells (n = 31/140), Chronos- and ChrimsonR-evoked EPSCs were pooled for specific inputs;

input-specific modulation by DA, 5-HT, METH, or MDMA did not depend on whether the opsin expressed in the input was Chronos or ChrimsonR.

Imaging. Images of injection sites were collected using a Nikon Instruments A1 Confocal Laser microscope (10× objective). For imaging, Chronos-mT-Sapphire 405-nm laser excitation was used with a GFP emission filter set. For ChrimsonR-LSSmOrange, an RFP emission filter set was used. Images were captured with NIS-Elements software and processed with ImageJ (NIH). No animals were excluded due to inaccurate injections.

Behavioral Assays. Juvenile interaction, 3-chamber sociability, novel object, and open-field (locomotor) assays were conducted as described (19). Laser stimulation (532-nm diode, Shanghai Dream Lasers Technology Co., Ltd.) was sent through an FC/PC adaptor and a fiber-optic rotary joint (Doric Lenses) to produce ∼15 mW light (measured by a digital power meter, Thorlabs) at the fiber tip. Laser output was controlled by a Master-8 pulse stimulator at a cycle of 8 s on and 2 s off during a given 10-s period. For all assays, the experimenter was blinded to the AAV injection (NpHR versus control eYFP) received by the mouse and remained blinded for analysis.

CPP test. Mice were brought to the testing room to habituate for 1 h before experiments began. Mice were placed in a rectangular Plexiglas arena with three chambers that could be separated by removable Plexiglas walls. The left and right chambers had distinct wall patterns (black and white stripes versus white with black circles) and flooring (distinct textured floors). The center chamber had no wall pattern and a smooth white floor. On day 1, a baseline preference was conducted. Subjects were placed in the center compartment for 2 min, at which point the barriers were lifted and the test mouse was allowed to freely explore the entire apparatus for 30 min. On days 2 through 4, two conditioning sessions were conducted per day, separated by at least 3 h using an unbiased design. On days 2 and 4, in the first session, the mouse was attached to the optical cables and confined to the one chamber, and the mouse was attached to the optical cables and confined to the designated unpaired chamber, without yellow-light stimulation, for 30 min; in the second session, the mouse was confined to the opposite, paired designated chamber with yellow-light stimulation (8 s on/2 s off) for 30 min. On day 3, the order of the sessions was reversed to account for any confounds due to time of conditioning. The stimulation-paired side was counterbalanced based on initial baseline preference. Mice that had a pretest preference of less than 0.3 or greater than 3 were excluded. The postconditioning test was conducted in the same manner as the baseline preference test on day 5.

Cocaine CPP was performed in the same manner as described in the preceding paragraph with the addition of an intraperitoneal injection of cocaine hydrochloride (5mg/kg, Tocris) immediately prior to the light stimulation session and an injection of saline prior to the "no light" session.

Juvenile interaction test. Mice were habituated for 1 min in their home cages (with cage mates temporarily placed in a different cage), during which the optical fiber cables were connected. Following habituation, a novel same-sex juvenile mouse (3 to 5 wk old) was introduced, and laser stimulation was applied for 2 min, during which free interaction was recorded with an overhead camera. Interaction time, defined as time the test mouse spent sniffing, actively pursuing, or grooming the juvenile, was subsequently analyzed manually and blindly. Individual social behaviors were not independently assayed. Mice underwent two rounds of the juvenile interaction assay separated by 1 h, and a novel juvenile was introduced during each session. Cohorts of mice were counterbalanced for the order of providing optogenetic stimulation versus no stimulation.

Three-chamber sociability test. On day 1, mice were habituated for 5 min to the arena in which an empty wire cup was placed in each of the outer chambers. Conspecific juveniles (3 to 5 wk old) of the same sex also were habituated to the cups. On day 2, test mice were introduced to the center chamber, and a conspecific juvenile was placed into one of the wire cups, the tops of which were covered to prevent mice from crawling on top. Placement of the juvenile mice in the chamber was counterbalanced across sessions. The wires in the cups formed a 0.8 × 0.8 cm mesh, and cups were immobilized in the centers of each of the side chambers. Test mice were placed in the center chamber for 2 min before barriers were raised to allow free exploration for 20 min. During each session, mice had 5 min epochs of the laser being off or on, which was counterbalanced across mice. Mouse location was assayed automatically with the video tracking software Biobserve. Sociability was calculated as follows: (time in juvenile side − time in empty side)/(time in juvenile side + time in empty side).

MDMA three-chamber sociability was performed in the same manner as described in the preceding paragraph with the addition of an intraperitoneal injection of MDMA (7.5mg/kg, Multidisciplinary Association for Psychedelic Studies) or saline, counterbalanced across NpHR and eYFP groups. The test was performed over 2 wk, with MDMA and saline also being counterbalanced for within animal comparison.

Novel object interaction test. This assay was performed exactly like the juvenile interaction assay, with either a toy mouse or plastic block instead of another mouse placed into the animal's home cage.

Open-field test (for locomotor activity). Mice were placed in a square arena (40 cm × 40 cm) and allowed to freely move for an 18-min session. During this session, mice had 3-min epochs of the laser being off or on, which was counterbalanced across mice. Total distance traveled and center time were automatically assayed using video tracking software (Biobserve) and compared between off and on epochs.

Data Analysis, Blinding, and Statistics. Investigators were always blinded to the manipulation that experimental subjects had received for behavioral assays. All electrophysiological and behavioral data were analyzed and graphed using GraphPad Prism 8. For electrophysiology assays, one-way analysis of variance (ANOVA), unmatched, with the Holm–Šidák correction for post hoc subgroup comparisons was used when multiple conditions were compared. For behavioral assays, two-way ordinary ANOVA with the Šidák correction post hoc was performed to compare multiple treatment conditions over multiple time points. Paired comparisons were performed when appropriate (e.g., before versus after conditioning; light off versus light on), and unpaired comparisons were used elsewhere. Electrophysiological data were tested for equal variances using the Brown–Forsythe test. All pooled data are expressed as mean ± SEM. For all experiments on the synaptic effects of DA, 5-HT, METH, and MDMA, an equivalent number of recordings for each input were obtained from male and female mice. For all behavioral experiments, each cohort consisted of approximately equal numbers of male and female mice. Similar levels of synaptic modulation were observed for both sexes, and therefore all electrophysiological results were pooled by input. There were also no significant differences in behavioral results, and therefore all mice were pooled by experimental condition.

Data Availability. AAV plasmids generated by this study are available from Addgene under the name of the lead contact. All study data are included in the article and/or supporting information.

ACKNOWLEDGMENTS. We thank members of the R.C.M. laboratory, Dr. Lu Chen, and Dr. Thomas Südhof for helpful comments on the project. We also thank Liliana King-Adas for technical support and the Stanford Neuroscience GVVC for supplying novel and stock viruses. This work was supported by the following grants: National Institute of Mental Health F32 MH115668 (to P.H.), National Institute of Diabetes and Digestive and Kidney Diseases K99 DK115895 (to D.J.C.), National Institute of Mental Health K08 MH110610 (to B.D.H.), National Institute on Drug Abuse P50 DA042012 (to R.C.M. and K.D.); by the University of California, San Francisco Dolby Family Center for Mood Disorders (to R.C.M. and K.D.); and by the Stanford University Wu Tsai Neurosciences Institute (to R.C.M.).

1. A. M. Klawonn, R. C. Malenka, Nucleus accumbens modulation in reward and aversion. *Cold Spring Harb. Symp. Quant. Biol.* **83**, 119–129 (2018).
2. G. J. Mogenson, D. L. Jones, C. Y. Yim, From motivation to action: Functional interface between the limbic system and the motor system. *Prog. Neurobiol.* **14**, 69–97 (1980).
3. P. O'Donnell, J. Greene, N. Pabello, B. L. Lewis, A. A. Grace, Modulation of cell firing in the nucleus accumbens. *Ann. N. Y. Acad. Sci.* **877**, 157–175 (1999).
4. S. J. Russo, E. J. Nestler, The brain reward circuitry in mood disorders. *Nat. Rev. Neurosci.* **14**, 609–625 (2013).
5. M. D. Scofield *et al*., The nucleus accumbens: Mechanisms of addiction across drug classes reflect the importance of glutamate homeostasis. *Pharmacol. Rev.* **68**, 816–871 (2016).
6. N. D. Volkow, R. A. Wise, R. Baler, The dopamine motive system: Implications for drug and food addiction. *Nat. Rev. Neurosci.* **18**, 741–752 (2017).
7. F. Ambroggi, A. Ishikawa, H. L. Fields, S. M. Nicola, Basolateral amygdala neurons facilitate reward-seeking behavior by exciting nucleus accumbens neurons. *Neuron* **59**, 648–661 (2008).
8. S. R. Sesack, A. A. Grace, Cortico-basal ganglia reward network: Microcircuitry. *Neuropsychopharmacology* **35**, 27–47 (2010).
9. Y. Zhu, C. F. R. Wienecke, G. Nachtrab, X. Chen, A thalamic input to the nucleus accumbens mediates opiate dependence. *Nature* **530**, 219–222 (2016).
10. G. D. Stuber *et al*., Excitatory transmission from the amygdala to nucleus accumbens facilitates reward seeking. *Nature* **475**, 377–380 (2011).
11. J. P. Britt *et al*., Synaptic and behavioral profile of multiple glutamatergic inputs to the nucleus accumbens. *Neuron* **76**, 790–803 (2012).
12. E. J. Van Bockstaele, V. M. Pickel, Ultrastructure of serotonin-immunoreactive terminals in the core and shell of the rat nucleus accumbens: Cellular substrates for interactions with catecholamine afferents. *J. Comp. Neurol.* **334**, 603–617 (1993).

13. B. W. Okaty, K. G. Commons, S. M. Dymecki, Embracing diversity in the 5-HT neuronal system. *Nat. Rev. Neurosci.* **20**, 397–424 (2019).
14. J. Ren *et al*., Anatomically defined and functionally distinct dorsal raphe serotonin sub-systems. *Cell* **175**, 472–487.e20 (2018).
15. E. E. Steinberg, P. H. Janak, Establishing causality for dopamine in neural function and behavior with optogenetics. *Brain Res.* **1511**, 46–64 (2013).
16. H. C. Tsai *et al*., Phasic firing in dopaminergic neurons is sufficient for behavioral conditioning. *Science* **324**, 1080–1084 (2009).
17. E. E. Steinberg *et al*., Positive reinforcement mediated by midbrain dopamine neurons requires D1 and D2 receptor activation in the nucleus accumbens. *PLoS One* **9**, e94771 (2014).
18. B. D. Heifets *et al*., Distinct neural mechanisms for the prosocial and rewarding properties of MDMA. *Sci. Transl. Med.* **11**, eaaw6435 (2019).
19. J. J. Walsh *et al*., 5-HT release in nucleus accumbens rescues social deficits in mouse autism model. *Nature* **560**, 589–594 (2018).
20. B. N. Mathur, N. A. Capik, V. A. Alvarez, D. M. Lovinger, Serotonin induces long-term depression at corticostriatal synapses. *J. Neurosci.* **31**, 7402–7411 (2011).
21. S. M. Nicola, J. Surmeier, R. C. Malenka, Dopaminergic modulation of neuronal excitability in the striatum and nucleus accumbens. *Annu. Rev. Neurosci.* **23**, 185–215 (2000).
22. N. X. Tritsch, B. L. Sabatini, Dopaminergic modulation of synaptic transmission in cortex and striatum. *Neuron* **76**, 33–50 (2012).
23. G. Dölen, A. Darvishzadeh, K. W. Huang, R. C. Malenka, Social reward requires coordinated activity of nucleus accumbens oxytocin and serotonin. *Nature* **501**, 179–184 (2013).
24. N. C. Klapoetke *et al*., Independent optical excitation of distinct neural populations. *Nat. Methods* **11**, 338–346 (2014).
25. K. K. Ade, Y. Wan, M. Chen, B. Gloss, N. Calakos, An improved BAC transgenic fluorescent reporter line for sensitive and specific identification of striatonigral medium spiny neurons. *Front. Syst. Neurosci.* **5**, 32 (2011).
26. S. M. Nicola, S. B. Kombian, R. C. Malenka, Psychostimulants depress excitatory synaptic transmission in the nucleus accumbens via presynaptic D1-like dopamine receptors. *J. Neurosci.* **16**, 1591–1604 (1996).
27. M. Muramatsu, M. D. Lapiz, E. Tanaka, J. Grenhoff, Serotonin inhibits synaptic glutamate currents in rat nucleus accumbens neurons via presynaptic 5-HT1B receptors. *Eur. J. Neurosci.* **10**, 2371–2379 (1998).
28. A. F. MacAskill, J. M. Cassel, A. G. Carter, Cocaine exposure reorganizes cell type- and input-specific connectivity in the nucleus accumbens. *Nat. Neurosci.* **17**, 1198–1207 (2014).
29. V. Pascoli *et al*., Contrasting forms of cocaine-evoked plasticity control components of relapse. *Nature* **509**, 459–464 (2014).
30. B. A. Grueter, A. J. Robison, R. L. Neve, E. J. Nestler, R. C. Malenka, ΔFosB differentially modulates nucleus accumbens direct and indirect pathway function. *Proc. Natl. Acad. Sci. U.S.A.* **110**, 1923–1928 (2013).
31. K. W. Lee *et al*., Cocaine-induced dendritic spine formation in D1 and D2 dopamine receptor-containing medium spiny neurons in nucleus accumbens. *Proc. Natl. Acad. Sci. U.S.A.* **103**, 3399–3404 (2006).
32. S. L. Jackman, W. G. Regehr, The mechanisms and functions of synaptic facilitation. *Neuron* **94**, 447–464 (2017).
33. S. M. Perez, D. J. Lodge, Convergent inputs from the hippocampus and thalamus to the nucleus accumbens regulate dopamine neuron activity. *J. Neurosci.* **38**, 10607–10618 (2018).
34. S. B. Floresco, C. D. Blaha, C. R. Yang, A. G. Phillips, Modulation of hippocampal and amygdalar-evoked activity of nucleus accumbens neurons by dopamine: Cellular mechanisms of input selection. *J. Neurosci.* **21**, 2851–2860 (2001).
35. C. Barrientos *et al*., Cocaine-induced structural plasticity in input regions to distinct cell types in nucleus accumbens. *Biol. Psychiatry* **84**, 893–904 (2018).
36. S. M. Nicola, R. C. Malenka, Dopamine depresses excitatory and inhibitory synaptic transmission by distinct mechanisms in the nucleus accumbens. *J. Neurosci.* **17**, 5697–5710 (1997).
37. S. M. Nicola, R. C. Malenka, Modulation of synaptic transmission by dopamine and norepinephrine in ventral but not dorsal striatum. *J. Neurophysiol.* **79**, 1768–1776 (1998).
38. J. Harvey, M. G. Lacey, A postsynaptic interaction between dopamine D1 and NMDA receptors promotes presynaptic inhibition in the rat nucleus accumbens via adenosine release. *J. Neurosci.* **17**, 5271–5280 (1997).
39. J. Harvey, M. G. Lacey, Endogenous and exogenous dopamine depress EPSCs in rat nucleus accumbens in vitro via D1 receptors activation. *J. Physiol.* **492**, 143–154 (1996).
40. R. B. Rothman, M. H. Baumann, Therapeutic and adverse actions of serotonin transporter substrates. *Pharmacol. Ther.* **95**, 73–88 (2002).
41. H. Higashi, K. Inanaga, S. Nishi, N. Uchimura, Enhancement of dopamine actions on rat nucleus accumbens neurones in vitro after methamphetamine pre-treatment. *J. Physiol.* **408**, 587–603 (1989).
42. M. Morales, E. B. Margolis, Ventral tegmental area: Cellular heterogeneity, connectivity and behaviour. *Nat. Rev. Neurosci.* **18**, 73–85 (2017).
43. M. K. Lobo *et al*., Cell type-specific loss of BDNF signaling mimics optogenetic control of cocaine reward. *Science* **330**, 385–390 (2010).
44. P. Kamilar-Britt, G. Bedi, The prosocial effects of 3,4-methylenedioxymethamphetamine (MDMA): Controlled studies in humans and laboratory animals. *Neurosci. Biobehav. Rev.* **57**, 433–446 (2015).
45. B. D. Heifets, R. C. Malenka, MDMA as a probe and treatment for social behaviors. *Cell* **166**, 269–272 (2016).
46. M. Corkrum *et al*., Dopamine-evoked synaptic regulation in the nucleus accumbens requires astrocyte activity. *Neuron* **105**, 1036–1047.e5 (2020).
47. A. Pinto, M. Jankowski, S. R. Sesack, Projections from the paraventricular nucleus of the thalamus to the rat prefrontal cortex and nucleus accumbens shell: Ultrastructural characteristics and spatial relationships with dopamine afferents. *J. Comp. Neurol.* **459**, 142–155 (2003).
48. G. D. Stuber, J. P. Britt, A. Bonci, Optogenetic modulation of neural circuits that underlie reward seeking. *Biol. Psychiatry* **71**, 1061–1067 (2012).
49. J. F. Cheer *et al*., Coordinated accumbal dopamine release and neural activity drive goal-directed behavior. *Neuron* **54**, 237–244 (2007).
50. O. M. Folkes *et al*., An endocannabinoid-regulated basolateral amygdala-nucleus accumbens circuit modulates sociability. *J. Clin. Invest.* **130**, 1728–1742 (2020).
51. E. A. Amadei *et al*., Dynamic corticostriatal activity biases social bonding in monogamous female prairie voles. *Nature* **546**, 297–301 (2017).
52. E. Lee *et al*., Enhanced neuronal activity in the medial prefrontal cortex during social approach behavior. *J. Neurosci.* **36**, 6926–6936 (2016).
53. H. E. Covington III *et al*., Antidepressant effect of optogenetic stimulation of the medial prefrontal cortex. *J. Neurosci.* **30**, 16082–16090 (2010).
54. M. Murugan *et al*., Combined social and spatial coding in a descending projection from the prefrontal cortex. *Cell* **171**, 1663–1677.e16 (2017).
55. W. N. Wayman, J. J. Woodward, Chemogenetic excitation of accumbens-projecting infralimbic cortical neurons blocks toluene-induced conditioned place preference. *J. Neurosci.* **38**, 1462–1471 (2018).
56. E. A. West, M. P. Saddoris, E. C. Kerfoot, R. M. Carelli, Prelimbic and infralimbic cortical regions differentially encode cocaine-associated stimuli and cocaine-seeking before and following abstinence. *Eur. J. Neurosci.* **39**, 1891–1902 (2014).
57. D. Sierra-Mercado, N. Padilla-Coreano, G. J. Quirk, Dissociable roles of prelimbic and infralimbic cortices, ventral hippocampus, and basolateral amygdala in the expression and extinction of conditioned fear. *Neuropsychopharmacology* **36**, 529–538 (2011).
58. J. P. Caballero, G. B. Scarpa, L. Remage-Healey, D. E. Moorman, Differential effects of dorsal and ventral medial prefrontal cortex inactivation during natural reward seeking, extinction, and cue-induced reinstatement. *eNeuro* **6**, ENEURO.0296-19.2019 (2019).
59. H. W. Berendse, Y. Galis-de Graaf, H. J. Groenewegen, Topographical organization and relationship with ventral striatal compartments of prefrontal corticostriatal projections in the rat. *J. Comp. Neurol.* **316**, 314–347 (1992).
60. J. M. Barker, J. R. Taylor, L. J. Chandler, A unifying model of the role of the infralimbic cortex in extinction and habits. *Learn. Mem.* **21**, 441–448 (2014).
61. J. J. Walsh, D. J. Christoffel, X. Wu, M. B. Pomrenze, R. C. Malenka, Dissecting neural mechanisms of prosocial behaviors. *Curr. Opin. Neurobiol.* **68**, 9–14 (2020).
62. L. Ye *et al*., Wiring and molecular features of prefrontal ensembles representing distinct experiences. *Cell* **165**, 1776–1788 (2016).
63. S. L. Scudder, C. Baimel, E. E. Macdonald, A. G. Carter, Hippocampal-evoked feedforward inhibition in the nucleus accumbens. *J. Neurosci.* **38**, 9091–9104 (2018).
64. D. M. Shcherbakova, M. A. Hink, L. Joosen, T. W. Gadella, V. V. Verkhusha, An orange fluorescent protein with a large Stokes shift for single-excitation multicolor FCCS and FRET imaging. *J. Am. Chem. Soc.* **134**, 7913–7923 (2012).